

Microstructure Observation and High-Temperature Property of Iron-Nickel-Base Superalloy

MING-YEN LI, SHIH-MING KUO and YEONG-TSUEN PAN

*New Materials Research & Development Department
China Steel Corporation*

The high-temperature mechanical properties and corresponding microstructure evolution of CSC's first iron-nickel-base superalloy product were investigated. The experimental results indicated that at the service temperature dispersive precipitation of TiC nanoparticles could be promptly brought out of Alloy 800H when fabricated through a specific production including ingenious alloy design, applicable electro-slag remelting and high-temperature solution-annealing. TEM observation showed that both the unique TiC and coexistent $M_{23}C_6$ precipitates are cubo-octahedral in shape and remain the cube-to-cube orientation relationship and coherent $\{111\}_{\text{carbide}/\gamma}$ and $\{100\}_{\text{carbide}/\gamma}$ interphase interface with austenite matrix, which bring about the dispersion-strengthening effect so that the time to rupture for the present alloy can be increased by 1.8 times in magnitude relative to the commercial heat-resistant product of the same grade. The improved creep property can be attributed to the mechanism that the nanometer-scale intragranular TiC and submicron intergranular $M_{23}C_6$ act as pinning points for individual dislocations and grain boundaries, resulting in the raised Orowan strengthening and suppressed grain boundary sliding at high temperature. Since the mentioned strengthening media are thermally stable and able to emerge readily prior to the formation of γ' phase, this work suggests an improved grade of superalloy for applications in a relatively harsh environment.

Keywords: Iron-nickel-base superalloy, Creep, Microstructure, Alloy 800H, TiC, $M_{23}C_6$

1. INTRODUCTION

Iron-nickel-base superalloy is one of the most widely used alloys in the energy and petrochemical industries. Heat-resistant Alloy 800H is the representative grade of iron-nickel-base superalloy, which provides a favorable combination of excellent creep properties, good resistance to high temperature oxidation, corrosion and carburization, and good structural stability at high temperatures⁽¹⁾. The material hence was recently recommended as a candidate material for the generation IV nuclear power plants⁽²⁾, bringing about more challenging conditions for its high-temperature applications. Since the creep resistance is the crucial property for use at temperatures above 593°C, Alloy 800H, containing a minimum 0.05 wt% C content, must be solution-annealed at a temperature higher than 1121°C to maintain a stable austenitic structure. The requirements of composition and annealing temperature promote a large stable grain size (ASTM No.5 or coarser) for better creep resistance. Beside, after a long serving time at temperature higher than 550°C, γ' precipitates tend to form due to Al + Ti content of 0.6 to 1.2 wt% in Alloy 800H. These precipitates can further

increase the creep resistance at temperature use up to 760°C. The time-temperature-transformation curves for the main precipitates in Alloy 800H can be reviewed in Fig.1.⁽³⁾ It is suggested, for certain temperature conditions such as at temperature higher than 650°C, a long incubation period for γ' is needed. In the serving condition of high loading at elevated temperatures, creep ruptures may occur before the emergence of γ' . In this case, to clarify the creep mechanism and microstructure evolution for 800H in the relatively harsh conditions become an important issue. It is worthwhile to build up a specific process which can bring about an alternative strengthening effect for extending industrial applications of the iron-nickel-base superalloy.

In this study, we report the high-temperature mechanical properties and corresponding microstructure evolution of CSC's first iron-nickel-base superalloy product, which suggest a grade-improved Alloy 800H strengthened by nanometre-scale carbide particles rather than γ' precipitates. The material was fabricated via the specific process so that the creep resistance can be improved. The creep mechanism of the strengthened alloy is also discussed.

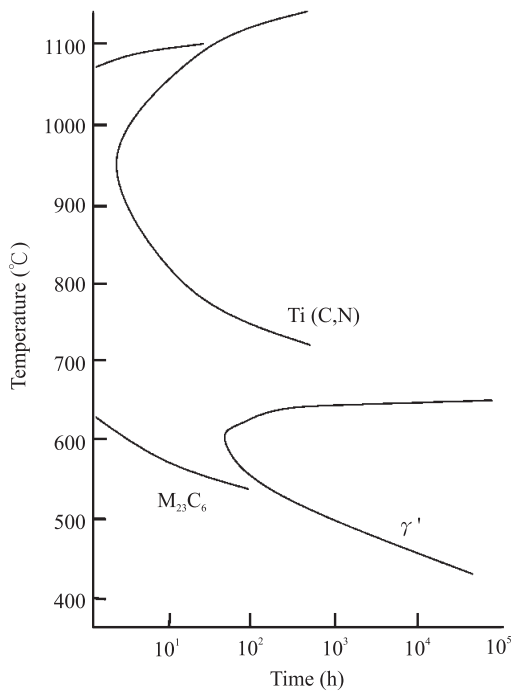


Fig.1. Time-temperature-transformation curves for the precipitates in Alloy 800H⁽³⁾.

2. EXPERIMENTAL METHOD

The compositions of the iron-nickel-base superalloy studied were based on Fe-46.5%, Ni-31.4%, Cr-20.1%, Mn-0.8%, Si-0.24, Cu-0.07%, Al-0.4% and a designed Ti:C ratio of 6.0 to 7.5⁽⁴⁾. The alloys were prepared by Argon Oxygen Decarburization (AOD) and then Electro-Slag Remelting (ESR) processes to 5-ton ingots. Hot forging and hot rolling were performed in China Steel Corporation's manufactory to form sheet coil of 6 mm in thickness. To control grain size, two

coils, ID# ESR-1 and ESR-2, were solution-annealed respectively at 1125 to 1160°C and 1160 to 1180°C for 30 min. The as-annealed grain size was measured to be 65 μm for ESR-1 and 107 μm for ESR-2. The high-temperature property was examined by the creep rupture tests at 650 and 705°C under a constant-load condition, and also by the short-time tensile test at temperatures from 30 to 850°C. The applied load of the rupture test corresponded to the initial tensile stress of 200 and 300 MPa. The test data of the present alloy were compared with those of the commercial 800H product, which was produced by a continuous-casting process with a lower Ti:C ratio of 4.0 to 5.0 (denoted as CC 800H). The morphology of the creep-ruptured samples were observed by scanning electron microscopy, (SEM, JEOL JSM-7500F) and the structure and distribution of the precipitates were analyzed by transmission electron microscopy (TEM, FEI E.O. Tecnai F20 G2 MAT S-TWIN).

3. RESULTS AND DISCUSSION

(1) Creep and tensile properties at high temperature

Figure 2 shows the time to rupture of the 800H samples corresponding to the various creep conditions tested in this study. It can be observed that creep temperature is a more sensitive factor than exerting stress on the creep lifetime of alloy 800H, and controlling the grain size is indeed an effective method to extend the time-to-rupture only when the temperature and/or stress conditions are not so severe. The alloys produced in this study obviously showed longer creep lives and better ductility than the commercial 800H product. For the case of ESR-2 at 650°C, the time to rupture was increased by 1.8 times in magnitude relative to the commercial creep-resistant product.

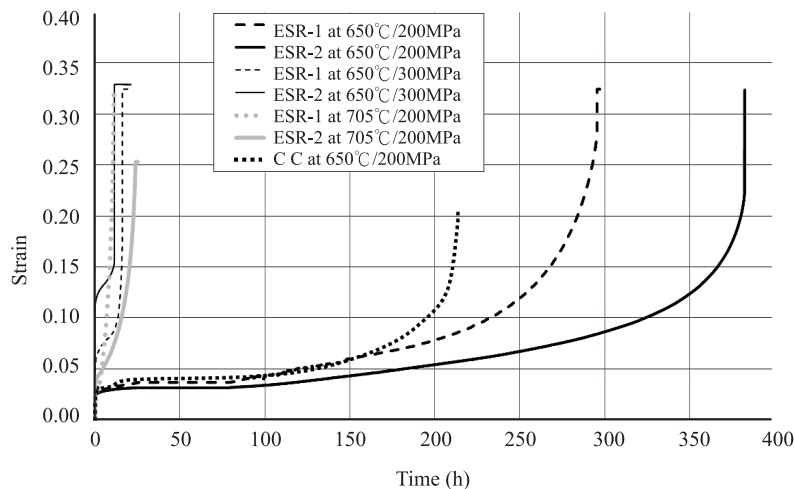


Fig.2. Time-to-rupture data for the iron-nickel-base superalloy investigated in this study.

On the other hand, the result of the tensile test also demonstrated that ESR-2 provided a superior short-time mechanical property on both sides of strength and ductility, as shown in Fig.3. It is leading the way on the short-time heat-resistant properties compared to the commercial 800H product at temperatures up to 705°C.

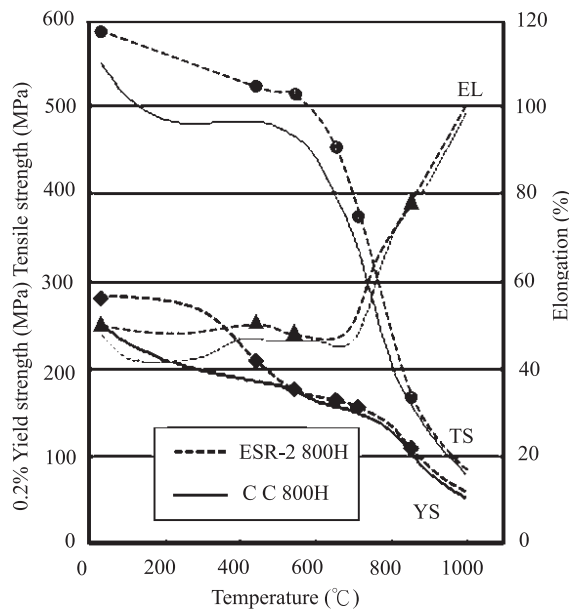


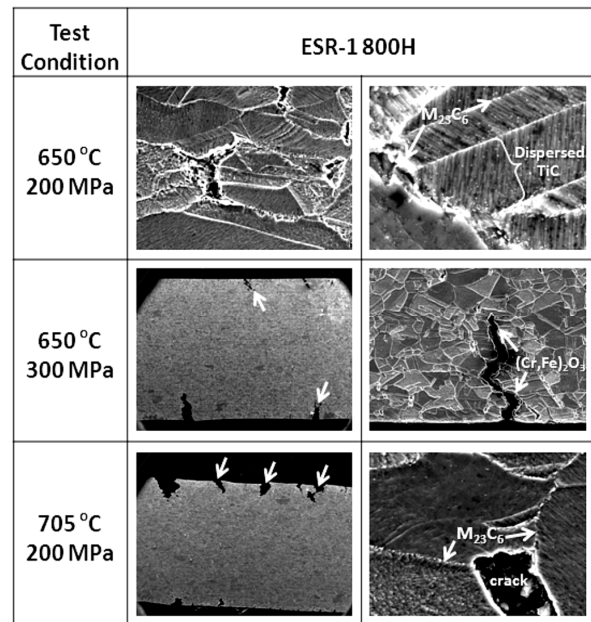
Fig.3. High-temperature tensile test data for the iron-nickel-base superalloy investigated in this study.

(2) SEM observation and creep mechanism

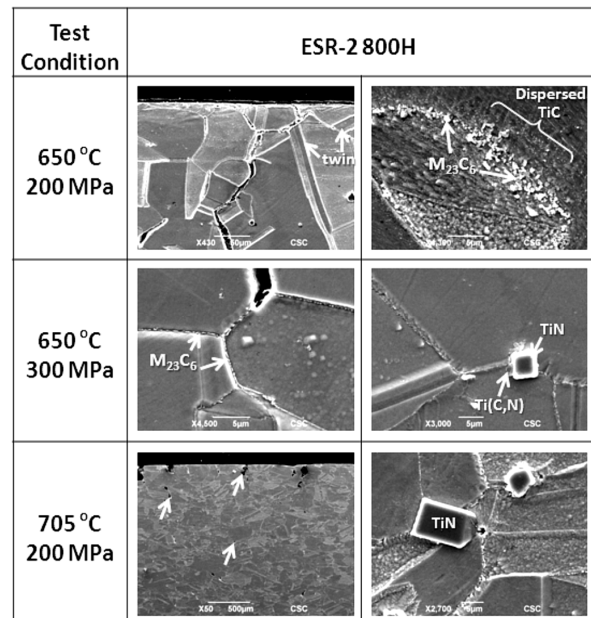
SEM observation on the stressed region of the stress-ruptured sample is shown in Fig.4, indicating the intergranular fracture behavior for the creep failure. Grain growth was not significant for all of the tested conditions. Increasing the testing stress or temperature would result in higher crack density and wider crack width. The precipitates formed at 650°C and 705°C were intragranular sphere-like TiC (0.1 to 0.5 μm in size), blocky TiN (5 to 20 μm in size), and intergranular Cr-rich $M_{23}C_6$ phase. Besides, it was observed that the twin density in austenitic structure was apparently increased after the creep deformation.

Generally, it is known that dislocation glide and grain boundary sliding lead to creep deformation at high temperature. Speculated from the SEM microstructure shown in Fig.4, the creep mechanism for the present alloy can be illustrated as in Fig.5. It is indicated that dislocations multiply inside austenite grains and pile up at grain boundaries. As a result, the cavities at austenite grain triple junctions would gradually form with the prolonged stress duration. Under the assistance of stress/thermal activated

grain boundary sliding, the cavities and cracks become easy to string up with each other and thus lead to the final rupture. It should be noted that the sample ESR-2 with larger grain size indeed has a longer rupture lifetime than the sample ESR-1 (Fig.2), suggesting that the diffusion or Coble creep may still play a considerable role in the high-temperature deformation.



(a)



(b)

Fig.4. Cross-sectional SEM images for (a) ESR-1 and (b) ESR-2 800H samples stress rupture-tested by the conditions noted on the left-hand side.

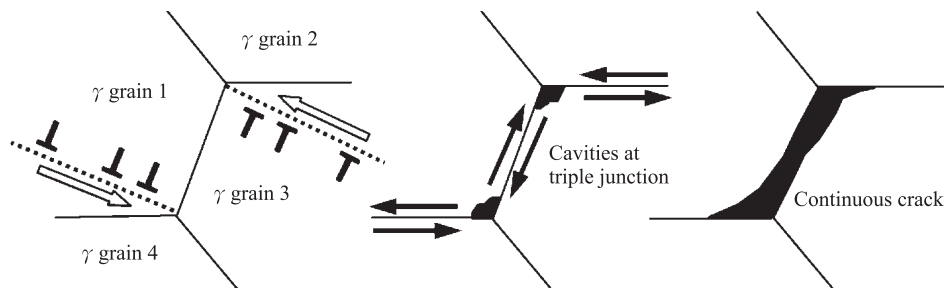


Fig.5. Schematic diagram (from left to right) for the creep rupture mechanism of the Alloy 800H studied.

- (3) TEM analysis and nanoprecipitates strengthening
 The creep rupture mechanism revealed in Fig.5 could be evidenced by the TEM observation of Fig.6, showing that dislocations tend to pile up at the grain and twin boundaries of austenite matrix during the stressed exposure at elevated temperatures. It was also observed that a considerable amount of $M_{23}C_6$ particles can be found at the grain and twin boundaries when the creep test was performed at 705°C (not shown). At 650°C, $M_{23}C_6$ also precipitated at dislocation but the particle size is smaller than those formed at grain boundary (Fig.7(a to c)). TiC phase, which was distributed intragranularly, was the main precipitate observed at 650 °C. The particle size of TiC was around 0.1 to 0.5 μm regardless of the creep conditions tested in this study. Nevertheless, secondary-precipitated TiC nanoparticles can be found in the austenite grain for the creep sample ESR-2, which showed the longest creep life time (Fig.7(d),(e)). High-Resolution TEM (HRTEM) analysis showed that the nano-sized TiC (Fig.8) and coexistent $M_{23}C_6$ (Fig.9) precipitates are both cubo-octahedral in shape, and remain the cube-to-cube orientation relationship and coherent $\{111\}_{\text{carbide}/\gamma}$ and $\{100\}_{\text{carbide}/\gamma}$ interphase interface with the austenite matrix. Analogous phase-transformation scenario of nano-size TiC precipitates cannot be found in the ruptured sample of the commercial CC 800H product even if the testing duration was extended over 1500 h for the low-stress condition (Fig.10). The observations on the precipitated particles might connect to the Orowan strengthening effect that the nanometer-scale intragranular TiC⁽⁵⁾ and the submicron intergranular $M_{23}C_6$ ⁽⁶⁾ can respectively act as pinning points for individual dislocations and grain boundaries, i.e., the enhanced creep resistance of the ESR 800H produced in this study can be attributed to the raised precipitate strengthening and suppressed grain boundary sliding. The current TEM observation also provided the supportive evidence for this kind of interaction between precipitate and dislocation, as shown in Fig.11.

The distinctive size and uniform dispersion of the

carbide particles found in this study should be related to the specific fabricating production of the sheet coil. In the first place, the alloy design for the Ti and C content and Ti:C ratio might had great influence on the precipitation degrees of TiC and $M_{23}C_6$ phases. Besides, the ESR process with the TiO_2 -contained slag⁽⁷⁾ could not only help to reduce the burning loss of the beneficial elements but also promoted the uniform solute distribution for the alloy slabs. In addition, the residual carbides formed during the melting and/or hot-working processes must be completely resolved by sufficient temperature/duration of solution-annealing to ensure the preferable precipitation behavior in service condition.

4. CONCLUSIONS

- (1) A grade-improved Fe-Ni-Cr-base superalloy, strengthened by nanometre-scale carbide particles rather than γ' precipitates, is reported in this study. The experimental results showed that the present alloy exhibited a time-to-rupture that is increased by 1.8 times in magnitude relative to the commercial creep-resistant product. Superior short-time tensile properties on both sides of high-temperature strength and ductility are also provided by the present alloy.



Fig.6. TEM BFI (Bright Field Image) of ESR-1 sample stress rupture-tested with 650°C/300 MPa condition, indicating the dislocations pile up at grain and twin boundaries of austenite matrix.

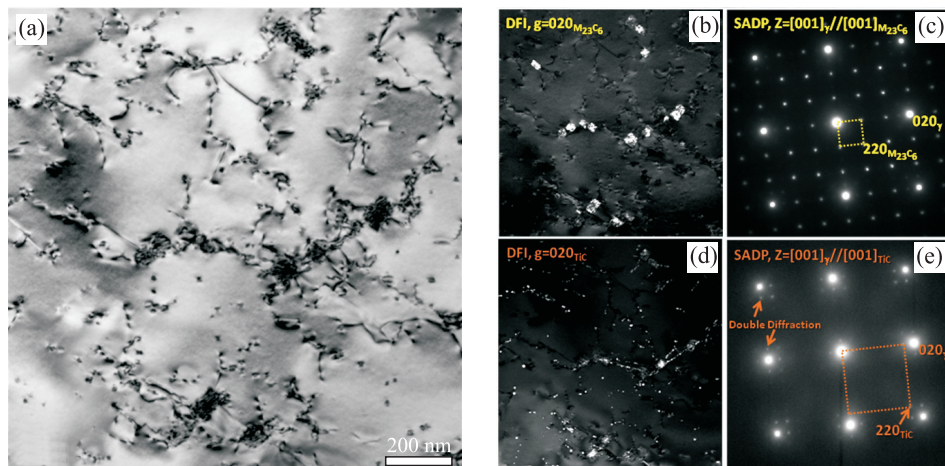


Fig.7. TEM images for sample ESR-2 rupture-tested with 650°C/200 MPa condition, showing the appearance of intragranular precipitates in austenite grain: (a) BFI, (b) DFI (Dark Field Image) and (c) SADP (Select Area Diffraction Pattern) of $M_{23}C_6$, (d) DFI and (e) SADP of TiC. The diffraction conditions of the DFI and SADP are noted in each image.

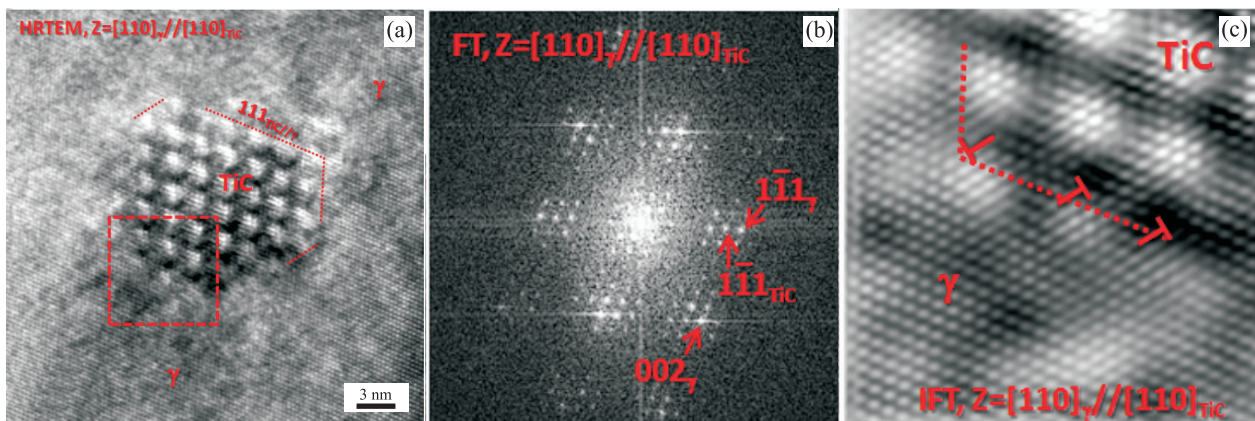


Fig.8. (a) HRTEM, (b) Two-dimensional Fourier transform (FT) and (c) Inverse transform (IFT) images for sample ESR-2 rupture-tested with 650°C/200 MPa condition, showing the TiC nanoprecipitate is cubo-octahedral in shape with cube-to-cube orientation relationship corresponding to the austenite (γ) matrix. Note the misfit dislocations (T) can be found at the coherent interphase interface. (b) and (c) were transformed from the square region in (a).

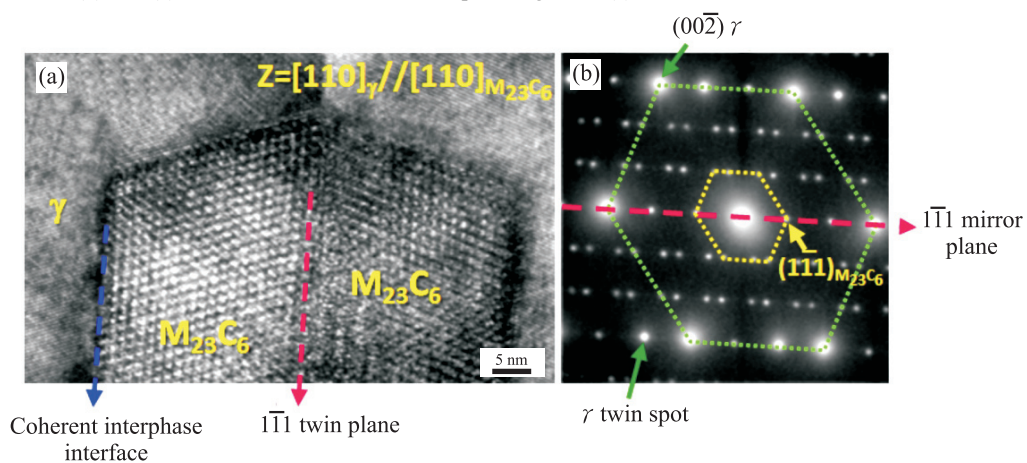


Fig.9. (a) HRTEM image and (b) Corresponding SADP ($Z=[110]_{\gamma}/[110]_{M_{23}C_6}$) of ESR-2 sample stress rupture-tested with 650°C/200 MPa condition, showing the $M_{23}C_6$ precipitated at the $(1\bar{1}1)_{\gamma}$ twin boundary, maintaining the twinning symmetry and the coherent interphase interface with matrix.

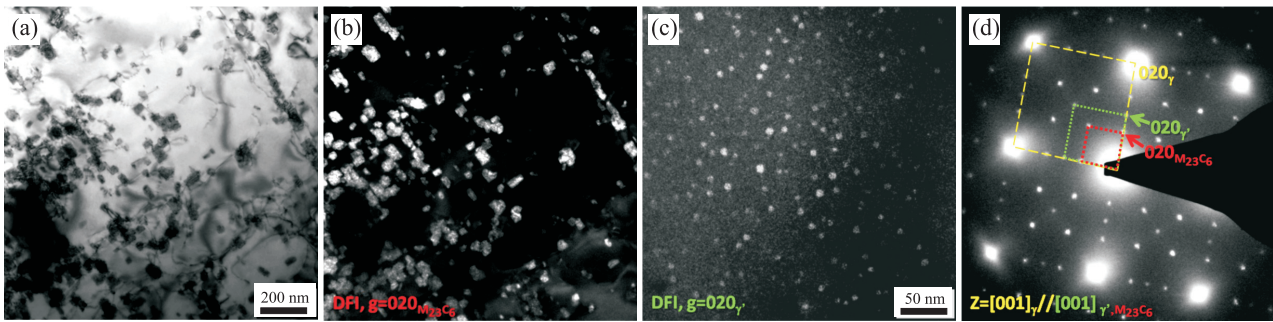


Fig.10. TEM images of C C 800H sample stress rupture-tested with 650°C/100 MPa condition, showing TiC is rarely found and the intragranular $M_{23}C_6$ and γ' are the main precipitated phases for creep lifetime longer than 1500 h: (a) BFI, (b) DFI of $M_{23}C_6$, (c) DFI of γ' and (d) SADP corresponding to (a)-(c), indicating the coexistent diffraction spots of $M_{23}C_6$, γ' and austenite matrix (γ). The diffraction conditions of the DFI and SADP are noted in each image.

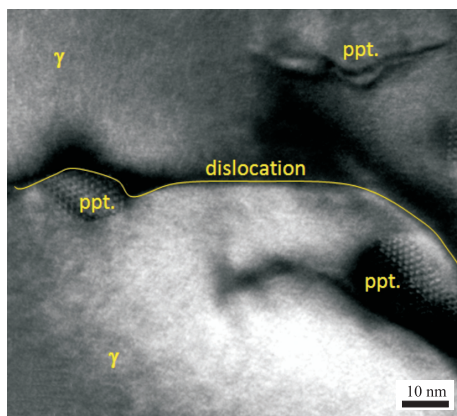


Fig.11. HRTEM image ($Z=[110]_{\text{ppt./}\gamma}$) of ESR-2 800H sample stress rupture-tested with 650°C/200 MPa condition, indicating the dislocations in γ were locally bent due to hindering of precipitates (denoted as ppt.).

(2) TEM observation on the stress-ruptured samples of the superalloy showed that both the TiC and $M_{23}C_6$ precipitates are cubo-octahedral in shape and remain the cube-to-cube orientation relationship and coherent $\{111\}_{\text{carbide}/\gamma}$ and $\{100\}_{\text{carbide}/\gamma}$ interphase interface corresponding to the austenite matrix. The improved properties can thus be attributed to the mechanism that the nanometer-scale

TiC and the submicron $M_{23}C_6$ act as pinning points for individual dislocations and grain boundaries, respectively.

(3) The particular microstructure evolution of present material occurring during creep can be connected to the specific production processes of alloy design, ESR and solution anneal developed in this study.

REFERENCES

1. W. Betteridge, R. Krefeld, H. Krockel, S. J. Lloyd and M. Van de Voorde, in *Alloy 800*, edited by C. Vivante (North Holland Publishing, New York, 1978).
2. W. Ren, in *A Review of Alloy 800H for Applications in the Gen IV Nuclear Energy Systems*, PVP2010-25727, Bellevue Washington (2010).
3. W. B. Jones and R. M. Allen, *Met. Trans. A*, 13, 637 (1982).
4. M. Y. Li, Y. T. Pan, I. T. Hong and S. M. Kuo, Proceedings of the 2012 Annual Conference of the Materials Research Society-Taiwan, Yunlin, Taiwan, Nov. 23-24th, 2012, pp. 2631-2634.
5. M. Taneike, F. Abe and K. Sawada, *Nature*, 424, 294 (2003).
6. A. Orlová, K. Milička and J. Čadek, *Mat. Sci. Eng. A*, 50, 221 (1981) and references cited therein.
7. C. Y. Chen et al, Internal Report TS-101001 in China Steel Corporation, 2012. □